Recovery of neutron-irradiated VVER-440 RPV base metal and weld exposed to isothermal annealing at 343°C up to 2,000 h

Eberhard Altstadt, Frank Bergner*, Jann-Erik Brandenburg, Paul Chekhonin, Jakub Dykas, Mario Houska and Andreas Ulbricht

Helmholtz-Zentrum Dresden-Rossendorf, Dresden, Germany

Neutron irradiation causes embrittlement of reactor pressure vessel (RPV) steels. Post-irradiation annealing is capable of partly or fully restoring the unembrittled condition. While annealing at high temperatures (e.g., 475°C) was successfully applied to extend the lifetime of operating VVER-440 reactors, the benefit of annealing at lower temperatures (e.g., 343°C—the maximum to which the primary cooling water can be heated) is a matter of debate. In this study, neutron-irradiated VVER-440 RPV base metal and weld were exposed to isothermal annealing at 343°C up to 2,000 h. Given the limited amount of material, the degree of recovery was estimated in terms of Vickers hardness, the ductile-brittle transition temperature derived from small punch tests, and the master curve reference temperature derived from fracture mechanics tests of mini samples. For the base metal, small-angle neutron scattering was applied to underpin the findings at the nm-scale. We have found significant partial recovery in both materials after annealing for 300 h or longer. The variations of the degree of recovery are critically discussed and put into the context of wet annealing.

KEYWORDS

reactor pressure vessel steel, embrittlement, wet annealing, recovery, hardness, small punch test, fracture mechanics, small-angle neutron scattering

1 Introduction

After a period of gradual decline of the global share of nuclear electricity generation, there are currently well-known advantages raising renewed interest in nuclear power (Dudarev, 2022). Lifetime extension of operating reactors is part of the story, with thermal recovery annealing of the reactor pressure vessel (RPV) being an option. The RPV is a critical component of nuclear power plants (NPP). On the one hand, neutron irradiation gives rise to a progressing shift of the ductile-brittle transition temperature (DBTT) of RPV steels towards higher temperatures (called embrittlement) (Ortner, 2023) raising the issue of safety of the RPV against brittle failure. On the other hand, the RPV is not economically replaceable (Ortner, 2023). Therefore, the embrittlement issue sets a limit to the lifetime of an RPV. One potential option to extend the lifetime is recovery annealing of the part of the RPV exposed to noticeable neutron irradiation at temperatures in excess of the operation temperature, the latter typically ranging between 260°C and 300°C for current pressurized water reactors.

From the technical point of view, two methods of recovery annealing were proposed and applied: dry annealing and wet annealing (Amayev et al., 1993; Mager et al., 1998; Pelli and Törrönen, 1998; Brumovsky et al., 2008; Brumovsky, 2015; Sokolov et al., 2015; Kryukov, 2019). For dry annealings carried out in the past, the RPVs were heated by electric-resistance radiant heaters arranged in the interior of the RPV. As a major advantage, dry annealing at suitable temperatures (e.g., 475°C) is capable of nearly restoring the DBTT of the unirradiated material (Brumovsky, 2015). Disadvantages of dry annealing are (1) the time and effort required to remove the fuels and internals from the reactor interior and to introduce the heating system and (2) the risk of exceeding the acceptable residual stress level in the RPV wall. The success of large-scale dry annealings applied to power reactors was demonstrated, in particular for VVER-440 type units (Ahlstrand et al., 1993; Pelli and Törrönen, 1998; Viehrig et al., 2009). For example, in 1988 dry annealing at a temperature of 475°C was applied to the RPV of NPP Greifswald Unit 1. The success of the annealing was shown using mini specimens prepared from shells of material, called boat samples, eroded from the inner RPV surface (Ahlstrand et al., 1993) before re-operation. This was later confirmed using standard samples prepared from trepans taken from the RPV wall after decommissioning of the unit (Viehrig et al., 2009).

Wet annealing (Fabry et al., 1984; Server and Biemiller, 1993; Pelli and Törrönen, 1998; Brumovsky et al., 2008; Krasikov, 2015; Kryukov, 2019) restricts the thermal annealing temperature to the design temperature of the nuclear steam supply system. In this process, the primary cooling water is heated up by means of the main circulation pumps with nuclear fission being stopped. This kind of heating the RPV is limited because of the simultaneously increasing, but also limited (by design), water pressure. A maximum temperature of 343°C can be reached in this way. Large-scale wet annealing of RPVs was reported occasionally. Primary coolant and nuclear heat (US Army SM-1A) or primary pump heat (Belgian BR-3) were applied to heat the RPV (Brumovsky et al., 2008). The annealing temperature in the former case was 293°C–300°C (service temperature 221°C). The degree of recovery was about 70% of the irradiation effect in terms of the transition temperature shift. In the BR-3 reactor, the service temperature was 260°C and the vessel was annealed at 343°C. The recovery was estimated to be at least 50%. The originally planned but not realized wet annealing of the Yankee Rowe vessel at 343°C (83 K above the service temperature) was predicted in the lab to give a 45%–55% recovery (Server and Biemiller, 1993).

According to Krasikov (2015), the recovery effect is vanishing for irradiation temperatures that are less than 70 K below the annealing temperature. Assuming a wet annealing temperature of approximately 340°C, the expected maximum irradiation temperature for noticeable recovery would be approximately 270°C. This is close to the typical irradiation temperature of VVER-440-type reactors. On the basis of experimental results (Amayev et al., 1993; Brumovsky et al., 2008), it was concluded that the expected effect of wet annealing at a temperature of 340°C would be too small to be considered as expedient for this type of reactors. However, a closer look at the reported results indicates a recovery of the transition temperature T_k of 20% on average (Amayev et al., 1993). More recently, lower levels of impurity Cu were reported to produce higher degrees of recovery after annealing

at 340°C (Kryukov, 2019). In conclusion, it is worth reconsidering the potential for partial recovery and possible lifetime extensions arising from wet annealing of VVER-440 RPVs taking into account an enhanced database and changed socio-economic factors, while maintaining necessary safety margins.

The present study aims at enhancing the database on the effect of annealing at a temperature of 343°C on the properties of neutron irradiated VVER-440-type RPV materials. Variations of the annealing time up to 2,000 h are included. The limited amount of available as-irradiated material requires small-specimen techniques to be favored over standard tests. From this point of view, we have decided to cover standard Vickers hardness tests, small punch tests (SPT) revealing information on the transition temperature shift, and fracture mechanics tests using small compact tension (C(T)) specimens. These methods are complemented by a microstructure study based on small-angle neutron scattering (SANS) with sensitivity to nm-sized irradiation-induced solute atom clusters.

2 Experiments

2.1 Materials

The materials originate from the RPVs of Units 4 and 8 of the NPP Greifswald, Germany. The RPV of Unit 4 represents the first generation of VVER-440/V230 NPPs, it was designed by OKB Gidropress and produced by Izhora in the former Soviet Union. Multilayer submerged arc welding was applied to assemble the forged rings of the RPV. The details of the welding process are reported elsewhere (Timofeev et al., 2010). Unit 4 was in operation from 1979 to 1990 for a total of 3208 effective days. After decommissioning of Unit 4 in 1990, trepans of diameter 119 mm were machined from the RPV wall of 150 mm thickness using a trepanning device equipped with a cutting tool consisting of four hard metal blades (Viehrig et al., 2018). The trepan in question originates from the beltline welding seam SN 0.1.4, the material designation is 10KhMFT. The samples in question referred to below as SG-4 were taken from slice No. 9 of the trepan representing a distance of 76 mm from the inner surface of the RPV wall. It is important to note that no unirradiated archive material is available from this welding seam.

The RPV of Unit 8 belongs to the second generation of VVER-440/V213 NPPs, it was produced by Škoda steel works (Czech Republic). Unit 8 was never put into service. Instead, the unirradiated RPV was cut into segments for dismantling. The samples of this study referred to below as GW-8 correspond to the RPV base metal of designation 15Kh2MFAA. These samples originate from segment B3.G1.8 representing the forged ring 0.3.1, which underwent the following heat treatment:

- Austenitization at 1,000°C followed by oil quenching,
- Tempering at 680°C–720°C followed by air cooling,
- Homogenization at 665°C for 31–90 h followed by furnace cooling,
- Stress relieving of the RPV after welding.

The compositions of the weld material SG-4 (10KhMFT) and the base metal GW-8 (15Kh2MFAA) introduced above are specified

TABLE 1 Results of analyses of 10KhMFT-type weld material SG-4 and 15Kh2MFAA-type base metal GW-8 in units of mass% (rest Fe).

	C	Mn	Si	Cr	Ni	Mo	V	P	Cu
SG-4	0.04	1.10	0.31	1.47	0.13	0.49	0.17	0.032	0.13
GW-8	0.15	0.45	0.30	2.86	0.10	0.79	0.31	0.008	0.05

in Table 1. The microstructure of GW-8 is bainitic. Material SG-4 exhibits an inhomogeneous microstructure typical of multilayer welds.

2.2 Samples

Using an electric discharge (EDS) machine, all specimens were cut from broken halves of previously tested unirradiated or as-irradiated Charpy-type samples (dimensions $10 \times 10 \times 55$ mm^3). The orientations of the tested samples with respect to the RPV were T-L and L-T for SG-4 and GW-8, respectively. For Vickers hardness testing, rectangular slices of dimensions $10 \times 10 \times 1$ mm^3 were cut. One side of these slices was mechanically ground and polished up to paper P1200 to remove the damage layer left by previous steps and guarantee a flat surface. The specimen dimensions used for Vickers hardness testing were also adopted for SANS experiments. In the case of SPT samples of area 10×10 mm^2, two EDS runs at slower feed rates were added to one side of the eroded samples in order to remove the shallow erosion layer introduced before and reach the required surface quality. The final thickness was (0.500 ± 0.005) mm. A drawing of the 0.16T-C(T) fracture mechanics specimens also eroded from broken halves of Charpy-type specimens is shown in Figure 1. Pre-cracks of a prospective length a_0 of approximately 4.0 mm were introduced

by means of resonance vibrations using the pulsator model Power Swingly 1 kN micro (SincoTec).

2.3 Neutron irradiation

As already mentioned, the samples of the weld material SG-4 were taken from the irradiated RPV of Unit 4 of NPP Greifswald after decommissioning and received their neutron exposure as a consequence of reactor operation (Viehrig et al., 2018). Samples of GW-8 were exposed to neutron-irradiation in the irradiation experiment NAP-2(C) using the BAGIRA irradiation rig at the research reactor of EK-CER Budapest, Hungary (Gillemot, 2010; Viehrig et al., 2010). The irradiation parameters experienced by the samples of this study are summarized in Table 2. Unirradiated reference samples are only available for GW-8.

2.4 Recovery annealing

Within this study, the samples were annealed under argon atmosphere using a single-zone tube furnace 13/50/200 (Carbolite Gero). A Eurotherm controller served for temperature control. The present study covers an annealing temperature of $(343 \pm 1)°$C and annealing times of 100, 300, 1,000, and 2,000 h followed by furnace cooling. Each of these annealing times was applied to samples envisaged for Vickers hardness testing, while, because of the limited volume of available material, only selected annealing times were applied to samples foreseen for the other applied methods as specified below.

In order to emulate the unirradiated reference condition of the weld material SG-4, an additional annealing at 475°C/152 h was included in the experimental program. It is known that this type of
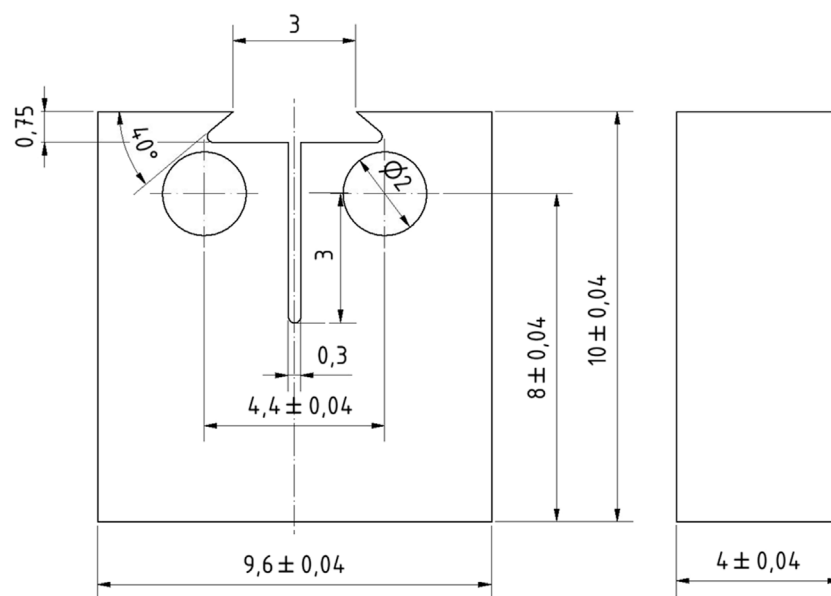

FIGURE 1
Drawing of the 0.16T-C(T) compact tension specimen for fracture mechanics testing. Dimensions given in mm.

TABLE 2 Irradiation conditions.

Material	Temperature (°C)	Irradiation time (days)	Fluence, E > 1 MeV (10^{19} n/cm^2)	Neutron flux, E > 1 MeV (10^{12} n/cm^{2}s)
SG-4	270	3207.9	1.073	0.0387
GW-8	290	48.75	11.7	27.8

annealing results in approximately 100% recovery (Ulbricht et al., 2011). Therefore, it is justified to use the post-irradiation annealed material as a substitute for the missing unirradiated weld material.

2.5 Methods

The Vickers hardness HV10 (load 98.1 N) was measured according to the standard ISO 6507 using a ZHU2.5 universal hardness testing machine (Zwick/Roell) equipped with an optical add-on unit. A hardness reference plate served as a means to regularly check correct calibration of the system. For each material and annealing condition, the average hardness was calculated (along with standard deviation) from 16 single Vickers hardness indentations placed sufficiently far away from each other to avoid interaction.

The small punch test (SPT) was applied to determine the ductile-to-brittle transition temperature (Altstadt et al., 2021) of irradiated steels. The main SPT parameters used are: punch diameter $d = 2.5$ mm, receiving hole diameter $D = 4$ mm, receiving hole edge chamfer 0.2 mm × 45°. The punch displacement v was measured by an inductive sensor with an accuracy of ±1 μm. The punch force was measured by means of a load cell placed between the puncher and the cross head of the electromechanical testing machine Inspekt 10 Desk (Hegewald & Peschke) with an accuracy of ±5 N. For each test, the force-displacement curve $F(v)$ was recorded and the small punch energy E_m was calculated as integral of $F(v)$ up to the maximum force F_m (Altstadt et al., 2021). The range of test temperatures from −160°C to 26°C was realized on the basis of liquid nitrogen cooling/resistance heating of the sample holder using a temperature control unit cRio (National Instruments). The ductile-to-brittle transition temperature (DBTT) T_{SP} was determined based on the normalized SP energy $E_n = E_m/F_m$ according to the standard EN 10371. The procedure includes the application of a tanh-fit to the data points $E_n(T)$. T_{SP} is defined as the temperature at which the fit curve reaches the average of the upper and lower shelf of the tanh-fit.

The master curve approach of brittle fracture mechanics (Wallin, 1999) was applied. For details on the use of mini-C(T) specimens we refer to Yamamoto and Miura (2015). Fracture mechanics testing of the pre-cracked 0.16T-C(T) specimens was performed in accordance with the standard ASTM E1921-21 using a servo-hydraulic test system MTS 810.21 (50 kN load capacity) equipped with a 10 kN load cell. The crack opening displacement was measured using a clip-on gage model 3541-005M-025M-LHT (Epsilon Technology) and converted into load-line displacement. The values of load and load-line displacement at crack instability along with the fractographically measured length of the pre-crack were used to calculate the elastic and plastic components of the J-integral, which was converted into the fracture toughness K_{Jc}. The test temperature was varied in the range from −130°C to −45°C such that sufficient numbers of valid tests according to the standard could be accumulated for each material condition. The K_{Jc} values measured for the used 0.16T-C(T) specimens were converted according to Equation 1 into equivalent $K_{Jc(1T)}$ values corresponding to standard 1T-C(T) specimens of 25.4 mm thickness (Yamamoto and Miura, 2015):

$$K_{Jc(1T)} = K_{min} + \left(K_{Jc} - K_{min}\right)\left(\frac{B}{B_{1T}}\right)^{1/4} \quad (1)$$

With $K_{min} = 20$ MPa$\sqrt{m}$, $B_{1T} = 25.4$ mm, and B the thickness of the samples, here $B = 4.0$ mm, Equation 1 reduces to $K_{Jc(1T)} = 7.4$ MPa$\sqrt{m} + 0.63K_{Jc}$. The reference temperature T_0 according to the master curve concept (Wallin, 1999), that means, the temperature at which $K_{Jc(1T)}$ reaches the level of 100 MPa$\sqrt{m}$, was determined by way of fitting Equation 2 to the $K_{Jc(1T)} - T$ dependence:

$$K_{Jc(med)} = 30 + 70 \cdot \exp\left[0.19\left(T - T_0\right)\right] \quad (2)$$

Using the same value of T_0, 2% and 98% tolerance bounds were calculated according to Equations 3 and 4, respectively. In Equations 2–4, the absolute terms and the pre-exponential factors are given in units of MPa$\sqrt{m}$.

$$K_{Jc(0.02)} = 24.1 + 29.0 \cdot \exp\left[0.19\left(T - T_0\right)\right] \quad (3)$$
$$K_{Jc(0.98)} = 35.5 + 108.3 \cdot \exp\left[0.19\left(T - T_0\right)\right] \quad (4)$$

The SANS experiments were carried out at the instrument D33 (Dewhurst et al., 2016) of the Institute Laue-Langevin (ILL) at Grenoble, France, using a neutron wavelength of 0.462 nm, a beam diameter of 8 mm and a sample-detector distance of 2 m. During the measurements a saturation magnetic field of 3 T oriented perpendicular to the neutron beam was applied to the samples. Absolute calibration was done using a water standard. The ILL software routines were applied to separate magnetic and nuclear scattering cross sections from the total cross sections as functions of the momentum transfer vector (also referred to as scattering vector) Q. The size distribution of scatterers was calculated by solving the inverse problem for the measured magnetic difference scattering curves (the scattering curve of the unirradiated condition taken as reference) using the indirect Fourier transform method (Glatter, 1980). Non-magnetic scatterers randomly dispersed in the ferromagnetic matrix were assumed as an approximation. Mean size, number density and volume fraction of scatterers were estimated supposing spherical shape. Finally, the average ratio of magnetic and nuclear scattering was calculated in terms of the so-called A-ratio, $A = 1 + M/N$, where M and N are the measured magnetic and nuclear difference scattering cross sections, respectively, both integrated over the relevant range of Q.

TABLE 3 Average Vickers hardness HV10 with standard deviation, derived Vickers hardness difference with respect to the unirradiated reference, and degree of recovery for base metal GW-8.

Condition	HV10	HV10-HV10$_\text{u}$	Recovery η (%)
Unirradiated	213.3 ± 2.2	n/a	n/a
Irradiated	253.7 ± 4.0	40.4 ± 4.6	n/a
Irradiated and annealed 100 h	246.2 ± 3.5	32.9 ± 4.1	19 ± 15
Irradiated and annealed 300 h	237.7 ± 2.5	24.4 ± 3.3	40 ± 16
Irradiated and annealed 1,000 h	226.5 ± 2.6	13.2 ± 3.4	67 ± 19
Irradiated and annealed 2000 h	222.6 ± 1.6	9.3 ± 2.7	77 ± 19

Although small-specimen test techniques such as the small punch test and fracture mechanics testing of mini-CT samples were applied, only subsets of the materials and annealing conditions were studied using the methods introduced above. This is mainly due to limited availability of unirradiated and as-irradiated material. Indeed, unirradiated archive material does not exist in the case of weld material SG-4 as already mentioned. Moreover, the weld takes up only the innermost fraction of the tested Charpy-type samples, typically 10–20 mm from the center (notch). The specimens of this study had to be prepared from this fraction. The final test matrix is summarized below:

- Vickers hardness testing: All as-irradiated and post-irradiation annealed (temperature 343°C, annealing times 100, 300, 1,000, and 2,000 h) conditions of both SG-4 and GW-8 are covered. Post-irradiation annealed (475°C/152 h) samples of SG-4 were tested to simulate the unirradiated reference.
- SPT: Unirradiated, as-irradiated, and post-irradiation annealed (343°C/100 and 1,000 h) conditions of GW-8 are covered.
- Fracture mechanics testing: Unirradiated, as-irradiated, and post-irradiation annealed (only 343°C/1,000 h) conditions of GW-8 are covered.
- SANS: Unirradiated, as-irradiated, and post-irradiation annealed (only 343°C/300 h) conditions of GW-8 are covered.

3 Results

3.1 Vickers hardness

The measured average Vickers hardness HV10 and its standard deviation are summarized in Table 3 for the base material GW-8. The results indicate the hardness to increase due to irradiation and to decrease at increasing annealing time as compared to the as-irradiated hardness. The latter effect is called recovery. The degree of recovery can be expressed as follows:

$$\eta = \left(1 - \frac{P_\text{ia} - P_\text{u}}{P_\text{i} - P_\text{u}}\right) \times 100\% = \frac{P_\text{i} - P_\text{ia}}{P_\text{i} - P_\text{u}} \times 100\% \qquad (5)$$

P is a property, here P = HV10. Subscripts u, i, and ia denote the unirradiated, as-irradiated, and post-irradiation annealed conditions, respectively. The hardness difference with respect to the unirradiated reference and the degree of recovery are included in Table 3.

As mentioned before, unirradiated archive material does not exist for the weld material SG-4. Therefore, the unirradiated reference was emulated on the basis of irradiated material exposed to a post-irradiation recovery annealing at 475°C/152 h. It was demonstrated beforehand (Ulbricht et al., 2011) that this kind of annealing gives rise to approximately 100% recovery, meaning that the annealed material serves as a good proxy of the unirradiated reference. Hence, the unirradiated condition in Equation 5 was replaced by the 475°C annealing in order to calculate the results for SG-4. The results are summarized in Table 4.

Figure 2A for GW-8 and Figure 2B for SG-4 illustrate the measured Vickers hardness plotted as function of the annealing time at 343°C. The values measured for the as-irradiated material and the unirradiated reference are shown as baselines. The plots indicate that:

- The irradiation-induced hardness increase is similar for both materials, ΔHV10 is approximately 40 and 45 for GW-8 and SG-4, respectively.
- The effect of post-irradiation annealing is significant for both materials except for the 100 h annealing of SG-4.
- There are trends of decreasing Vickers hardness, that means increasing recovery, as function of annealing time for both materials.
- There is no clear saturation of the hardness recovery within the covered range of annealing time.
- The hardness level of the unirradiated reference, that means 100% recovery, is not reached within the covered range of annealing time.
- The degree of recovery found for GW-8 is significantly larger (approximately by a factor of 2) than for SG-4.

3.2 Small punch test

The results of the individual small punch tests carried out for the base metal GW-8 are plotted in Figure 3 in terms of normalized SP energy versus test temperature. The best-fit tanh-curves are also plotted. The SPT-based ductile-brittle transition temperatures T_SP derived from the tanh-fits are summarized in Table 5. The errors are the result of the application of a Monte Carlo procedure (Urwank, 1989). The results indicate a significant irradiation-induced shift of the DBTT towards higher temperatures and significant effects of annealing. The degree of recovery consistent with Equation 5 is 28% and 35% for annealing durations of 100 and 1,000 h, respectively.

TABLE 4 Average Vickers hardness HV10 with standard deviation, derived Vickers hardness difference with respect to the approximate unirradiated reference, and degree of recovery for weld SG-4.

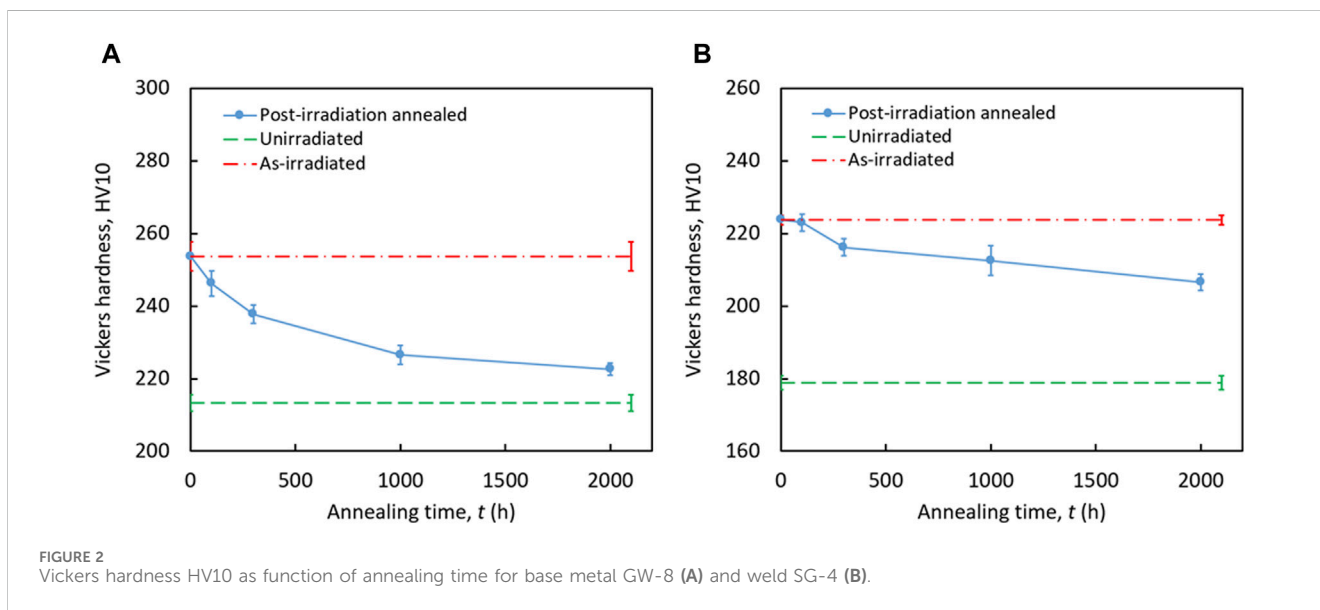| Condition	HV10	HV10-HV10$_u$	Recovery η (%)
Unirradiated (approximate)	178.9 ± 1.9	n/a	n/a
Irradiated	223.7 ± 1.3	44.8 ± 2.3	n/a
Irradiated and annealed 100 h	223.0 ± 2.4	44.1 ± 3.1	2 ± 6
Irradiated and annealed 300 h	216.2 ± 2.3	37.3 ± 3.0	17 ± 7
Irradiated and annealed 1,000 h	212.5 ± 4.1	33.6 ± 4.5	25 ± 11
Irradiated and annealed 2000 h	206.5 ± 2.3	27.6 ± 3.0	38 ± 8

FIGURE 2
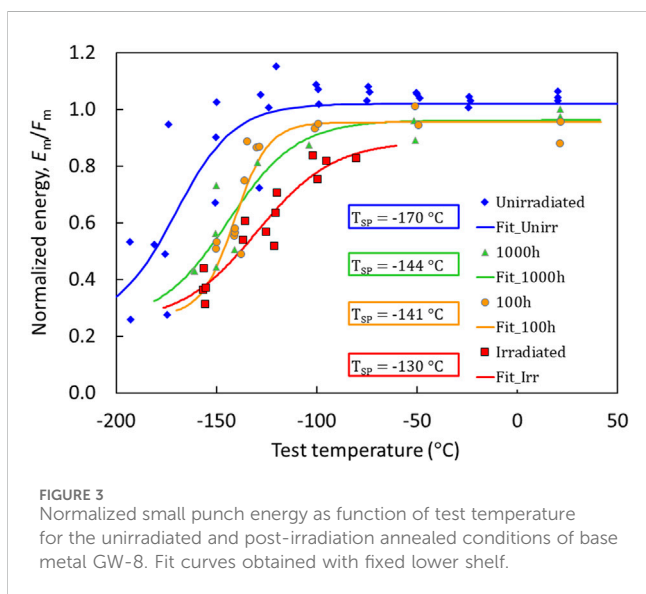Vickers hardness HV10 as function of annealing time for base metal GW-8 (A) and weld SG-4 (B).

FIGURE 3
Normalized small punch energy as function of test temperature for the unirradiated and post-irradiation annealed conditions of base metal GW-8. Fit curves obtained with fixed lower shelf.

The difference between the 100-h and 1000-h annealings is not significant. Interestingly, the slopes of the fitted curves for the two annealings differ considerably.

3.3 Fracture mechanics

The results of the fracture mechanics tests are shown in Figure 4 for the unirradiated (A), the as-irradiated (B), and the post-irradiation annealed conditions (C) of base metal GW-8. The measured data are indicated as symbols. Circles and triangles represent valid and invalid results, respectively, according to the standard. The validity window is enclosed by dotted lines. The dashed lines obtained by fitting (parameter T_0) are the median K_{Jc}-T curves according to Equation 2. The solid lines enclose the 2%–98% probability range. The results summarized in Table 6 indicate a significant irradiation-induced increase of the master curve reference temperature T_0 and a significant annealing effect. Taking into account experimental errors, a minimum recovery of 50% and a mean value of recovery close to 100% were observed.

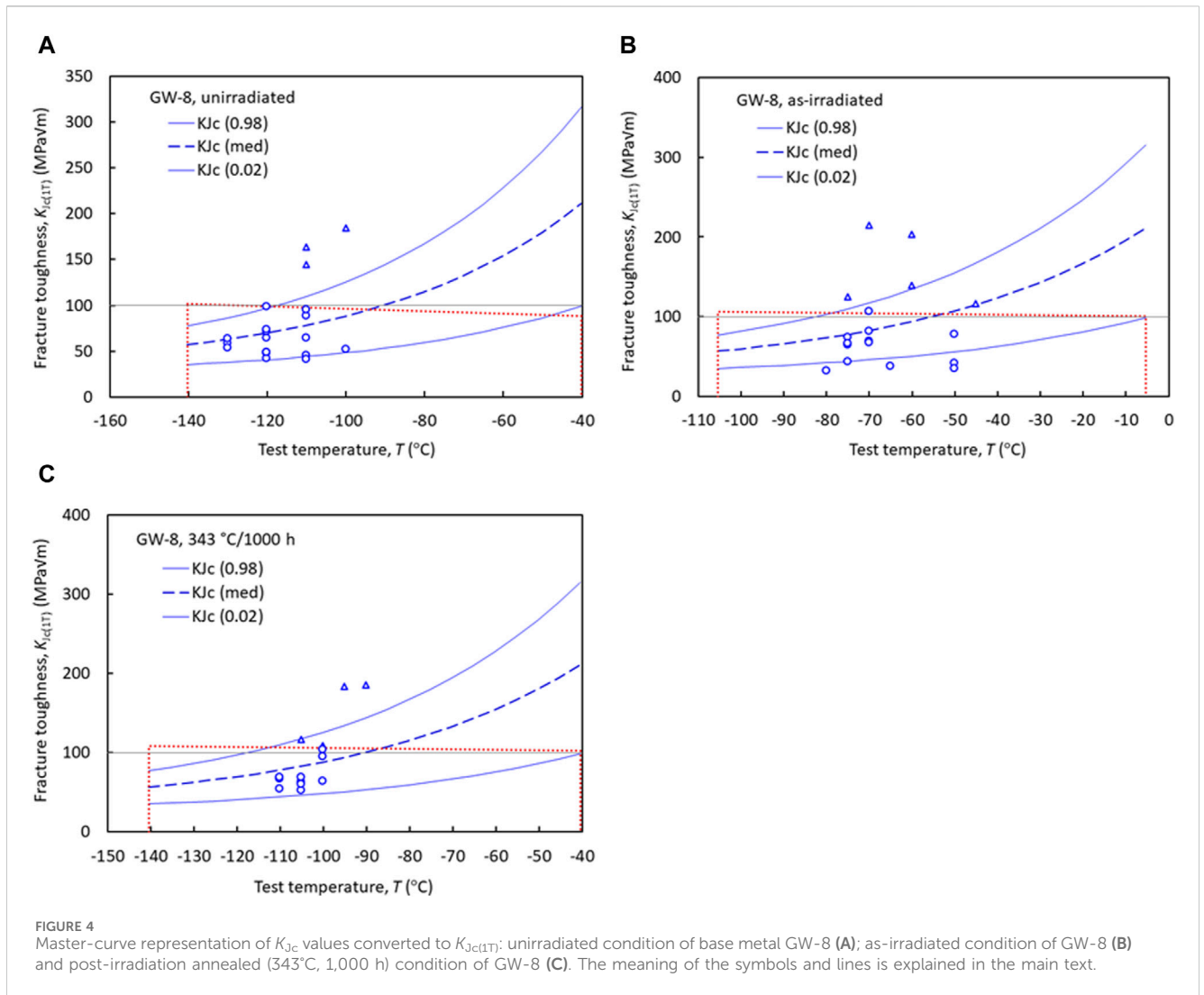## 3.4 Small-angle neutron scattering

The measured total, nuclear and magnetic scattering cross sections of the unirradiated, as-irradiated and post-irradiation annealed conditions of base metal GW-8 are plotted in Figure 5A as functions of the scattering vector Q. The separated magnetic scattering cross
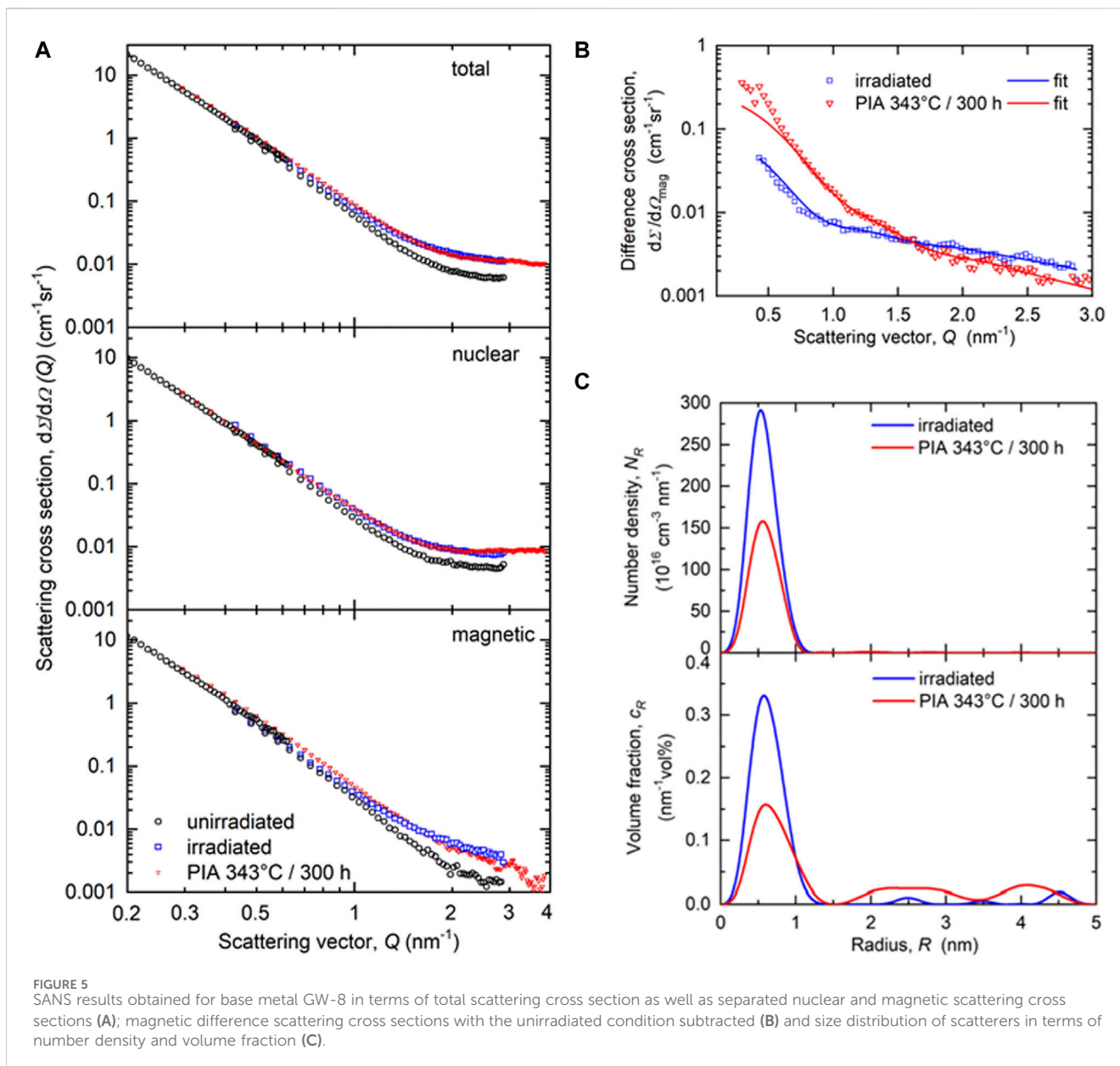
TABLE 5 Transition temperature T_{SP} from the SPT with standard deviation, difference with respect to the unirradiated reference, and degree of recovery for base metal GW-8.

Condition	T_{SP} (°C)	$T_{SP}-T_{SP,u}$ (K)	Recovery η (%)
Unirradiated	−170 ± 4	n/a	n/a
Irradiated	−130 ± 5	40 ± 7	n/a
Irradiated and annealed 100 h	−141 ± 3	29 ± 5	28 ± 17
Irradiated and annealed 1,000 h	−144 ± 5	26 ± 7	35 ± 22

TABLE 6 Master-curve reference temperature T_0 with standard deviation, difference with respect to the unirradiated reference, and degree of recovery for base metal GW-8.

Condition	T_0 (°C)	$T_0-T_{0,u}$ (K)	Recovery η (%)
Unirradiated	−90.3 ± 6.1	n/a	n/a
Irradiated	−55.4 ± 6.4	35 ± 9	n/a
Irradiated and annealed 1,000 h	−90.4 ± 6.9	0 ± 10	100 ± 50

FIGURE 4
Master-curve representation of K_{Jc} values converted to $K_{Jc(1T)}$: unirradiated condition of base metal GW-8 **(A)**; as-irradiated condition of GW-8 **(B)** and post-irradiation annealed (343°C, 1,000 h) condition of GW-8 **(C)**. The meaning of the symbols and lines is explained in the main text.

FIGURE 5
SANS results obtained for base metal GW-8 in terms of total scattering cross section as well as separated nuclear and magnetic scattering cross sections **(A)**; magnetic difference scattering cross sections with the unirradiated condition subtracted **(B)** and size distribution of scatterers in terms of number density and volume fraction **(C)**.

sections were used to determine the magnetic difference scattering curves in Figure 5B with the unirradiated condition taken as reference. The fit lines in Figure 5B are the Fourier counterparts (Glatter, 1980) of the size distributions shown in Figure 5C in terms of the number density and volume fraction of irradiation-induced clusters. For absolute calibration, the scatterers were assumed to be non-magnetic (magnetic holes).

The mean radius of solute atom clusters that were formed during irradiation and survived after annealing was found to be (0.6 ± 0.1) nm. The average ratio A of total (= nuclear + magnetic) and magnetic difference scattering cross sections is 1.8 ± 0.1 and 2.0 ± 0.1 for the as-irradiated and post-irradiation annealed conditions, respectively. The results indicate a significant amount of irradiation-induced clusters in terms of both volume fraction and number density and a reduction of the number density of clusters as a result of the annealing at 343°C/300 h. The size distribution in terms of volume fraction in Figure 5C also indicates coarsening of part of the clusters. The apparent difference between the two representations of

the size distribution at radii larger than 1.5 nm is due to the fact that coarser clusters contribute more to the volume fraction (third power of size) but less to the number density. The integrated total volume fractions c and number densities N of clusters as well as their respective degrees of recovery are listed in Table 7. It is important to note that the volume fraction of irradiation-induced clusters in the unirradiated condition is zero by definition.

The degree of recovery obtained by applying the different experimental methods to base metal GW-8 is summarized in Table 8. We have found that each method indicates a significant partial recovery for each of the covered annealing times. The individual statistical errors of the degree of recovery are relatively large and there is a pronounced scatter from method to method. Methods applied to samples exposed to the same annealing time (100, 300 or 1,000°C) still give consistent results in the sense that the error ranges derived from the standard deviations of the measured quantities do overlap.

TABLE 7 Total volume fractions c and total number densities N of solute atom clusters in base metal GW-8 as well as their respective degrees of recovery.

Condition	c (vol%)	Recovery η (%)	N (cm^{-3})	Recovery η (%)
Irradiated	0.19 ± 0.02	n/a	136 ± 15	n/a
Irradiated and annealed 300 h	0.15 ± 0.02	21 ± 17	78 ± 8	43 ± 17

TABLE 8 Degrees of recovery derived from the application of different characterization methods for the annealing times covered in the present study (base metal GW-8).

Method	Annealing time (h)	Recovery η (%)
Vickers hardness (ΔHV10)	100	19 ± 15
	300	40 ± 16
	1,000	67 ± 19
	2000	77 ± 19
SPT (ΔT_{SP})	100	28 ± 17
	1,000	35 ± 22
Fracture mechanics (ΔT_0)	1,000	100 ± 50
SANS (c)	300	21 ± 17
SANS (N)	300	43 ± 17

4 Discussion

For the 15Kh2MFAA-type RPV base metal GW-8 annealed at 343°C, each of the applied methods indicates a significant post-irradiation annealing effect, that means, a significant shift of the respective experimental quantity from its value in the as-irradiated condition towards its value in the unirradiated condition, so-called recovery. Despite the relatively large experimental errors of the degree of recovery it is worth considering the trends and comparing the values derived from different methods. First of all, all cases with variations of the annealing time (Vickers hardness and SPT) indicate a trend of the recovery increasing with increasing annealing time. A saturation of this trend towards a constant degree of recovery at increasing annealing time was not observed up to 2,000 h, but cannot be excluded because of the errors. A further extension of the annealing time was not feasible owing to the multi-purpose use of the furnace. Moreover, annealing times beyond 2,000 h are probably irrelevant from the viewpoint of practical feasibility in NPPs for economical reasons.

A comparison of the degrees of recovery obtained by means of Vickers hardness testing, (19 ± 15)%, and SPT, (28 ± 17)%, for the annealing time of 100 h indicates rough agreement rather than a trend. Similar implications are applicable for the annealing time of 1,000 h, for which Vickers hardness, SPT, and fracture mechanics testing indicate degrees of recovery of (67 ± 19)%, (35 ± 22)%, and (100 ± 50)%, respectively. However, it is worth noting that both ΔT_{SP} derived from the SPT and ΔT_0 derived from fracture mechanics testing may include contributions of non-hardening embrittlement (e.g., caused by phosphorous segregation to grain boundaries), which do not manifest themselves in the values of ΔHV10. Such contributions can neither be confirmed nor excluded on the basis of the present results. With respect to the recovery in terms of T_0, we suspect that the real recovery is closer to the lower limit of 50% than to
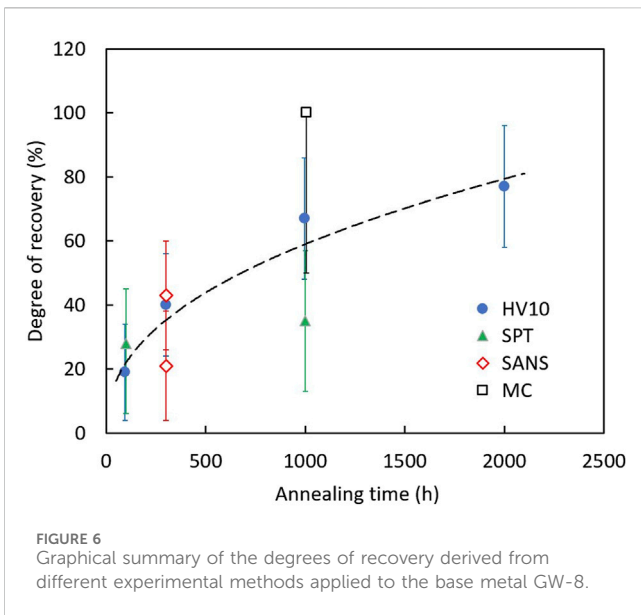
the mean value of 100%, such that consistency with the recovery derived from the SPT (maximum of 57%) is given. Indeed, ductile-brittle transition temperature shifts and shifts of the master curve reference temperature are frequently reported to be correlated (Viehrig et al., 2002; Nanstad et al., 2018; Altstadt et al., 2021), which would imply equal degrees of recovery in the present context.

An interesting aspect of the SANS results is the dominant type of detected irradiation-induced nanofeatures. Among the nanofeatures known to form in neutron-irradiated RPV steels, Cu clusters exhibiting A-ratios much larger than 2 (Mathon et al., 1997) can be excluded because of the measured A-ratio, $A = 2.0$ and $A = 1.8$ for as-irradiated and post-irradiation annealed GW-8 as well as the low Cu content of GW-8. A dominance of vacancy clusters exhibiting an A ratio of $A = 1.4$ (Bergner et al., 2008) can also be excluded. A low number density of dislocation loops may be present (Kocik et al., 2002), but does not give rise to significant SANS cross sections because of negligible SANS contrast (Bergner et al., 2008). Instead, the SANS observations are consistent with Mn-Ni-Si-enriched clusters (Almirall et al., 2019) as the dominant type of nanofeatures that formed under irradiation or survived after annealing. For VVER440-type RPV steels, these clusters may also contain Cr, which is not present in western-type RPV steels.

The difference between the degrees of recovery obtained by SANS for an annealing time of 300 h (based on ether number density of volume fraction of clusters) can be understood as a result of the different roles of cluster size in the calculations of number density and volume fraction. As already mentioned above, there is an increase of the volume fraction of larger clusters (radii between 1.5 and 5 nm, see Figure 5C) as a result of annealing. The effect of these larger clusters is overrepresented in the volume fraction, which contains size to the third power, but comparatively underrepresented in the number density. The latter gives rise to an apparently larger degree of recovery. If we compare the average value of 32% with the degree of recovery derived from Vickers hardness testing and SPT, we observe reasonable agreement.

The whole set of data for GW-8 listed in Table 8 is graphically summarized in Figure 6. Different symbols stand for different experimental methods applied to estimate the degree of recovery. The dashed line does not represent any model or physically based trend line equation. Instead, it indicates that none of the experimental points is an outlier from a purely statistical point of view. In spite of considerable scatter, the whole set of data is statistically consistent with respect to a common trend.

A comparison of the recovery observed by Vickers hardness testing for the base metal GW-8 and the weld material SG-4 is particularly important, because the neutron embrittlement of the weld located in the beltline region of the RPV is the dominant factor that limits the lifetime of the RPV. In the present case, the weld material is particularly meaningful, as it was directly taken from the beltline region of a real RPV. Therefore, both neutron flux and irradiation temperature are representative of the real situation. Instead, the externally irradiated base metal of the present study was exposed to a higher irradiation temperature (290°C instead of 270°C) and a three orders of magnitude higher neutron flux.

FIGURE 6
Graphical summary of the degrees of recovery derived from
different experimental methods applied to the base metal GW-8.

Most importantly, the degree of recovery in terms of Vickers hardness obtained for weld material SG-4 (Table 4) is significantly larger than zero except for the shortest annealing time of 100 h. This indicates a significant recovery. Comparing this degree of recovery with the base metal GW-8 (Table 3), we have found a significantly lower recovery for the weld. There are three potential sources of this difference: material/microstructure, irradiation temperature, and neutron flux. Little can be said here about the effect of the material, because the composition and microstructure of the base metal and weld are different in several respects, see Section 2.1. The higher phosphorus content in SG-4 may result in a higher fraction of non-hardening embrittlement. The higher copper content of SG-4 may give rise to a smaller degree of recovery at 343°C (Kryukov, 2019). With respect to the irradiation temperature, 270°C for the weld as compared to 290°C for the base metal, it is expected for otherwise equal conditions that the higher difference between the temperatures of annealing and irradiation would give rise to a more pronounced recovery in the weld. This is obviously not the case in our study. It can be concluded that the irradiation temperature is not the dominating factor here. Finally, the three orders of magnitude higher neutron flux experienced by the base metal GW-8 is expected to give rise to a significantly larger fraction of so-called unstable matrix defects (Odette and Lucas, 1998) of unspecified nature in addition to more stable solute atom clusters. By definition, an annealing at 343°C removes most of the unstable matrix defects and reverses the hardening that resulted from it. In general, higher flux tends to produce more unstable matrix defects. At the same time, a smaller difference between annealing and irradiation temperature tends to remove a higher fraction of unstable matrix defects as compared to solute atom clusters. It can be tentatively concluded that the more efficient recovery of the base metal as compared to the weld material is due to the much higher neutron flux.

After the discussion of the results obtained within this study it is interesting to consider the observations in the broader context of reported results. In an early basic study (Pachur, 1982), reported the

Vickers hardness of a neutron-irradiated A533B-type RPV steel (irradiation temperature 290°C) as function of the post-irradiation annealing time for isothermal annealing at 400°C. This author found a decrease of the Vickers hardness for annealing times below 2 h [stage 3 in Pachur (1982)] followed by a slight increase or plateau of the hardness and a further decrease in the range between 7 and 25 h [stage 4 in Pachur (1982)]. It was possible to attribute an Arrhenius-type of behavior with activation energies of 1.86 eV and 2.05 eV to stages 3 and 4, respectively, indicating different mechanisms of recovery and different types of irradiation-induced defects. However, the study was unspecific about these mechanisms and types of defects. The results of the present study can be compared with the reported results realizing that the lower annealing temperature of 343°C instead of 400°C is compensated by much longer annealing times up to 2,000 h instead of 25 h. While the investigated base metal GW-8 does not show such a two-stage behavior in the considered range of annealing times, the results obtained for the weld material SG-4 might be consistent with the operation of two different stages. Beyond this, the framework of empirical stages applied to the present results does not seem to generate further insight.

A comprehensive study on the annealing behavior at 340°C of neutron-irradiated (temperature 270°C, different fluences) VVER-440 base metals and welds was reported by Amayev et al. (1993) in terms of the Charpy-V transition temperature shift ΔTT [see also (Brumovsky et al., 2008)]. The annealing time selected for that study was 150 h. The average recovery of ΔTT was found to be approximately 20% with a wide range of scatter from 0% to 36% depending on both the neutron fluence and the type of material (base metal versus weld), weld material exhibiting the lower degrees of recovery between 0% and 20%. The present dependence of the recovery in terms of Vickers hardness on the annealing time indicates that at increasing time the degree of recovery tends to increase to beyond the values reported by Amayev et al. (1993) suggesting the possible efficiency of long-term wet annealing of VVER-440 RPVs. Taking notice of the correlations with ΔTT, this is also confirmed by the degrees of recovery of ΔT_{SP} and ΔT_0 observed for 1,000 h. Another important aspect is the effect of the level of impurity copper, which is lower for GW-8 as compared to the RPV steels studied by Amayev et al. (0.05% versus ~0.12%). Indeed, an increasing Cu content was reported to result in a trend of the degree of recovery after annealing at 340°C to decrease, at least at Cu contents beyond 0.2% (Kryukov, 2019).

In other studies, the annealing behavior of Cu-containing A533B cl. 1 RPV steels JRQ (forging, 0.15% Cu) and JPA (plate, 0.29% Cu) (Ulbricht et al., 2006) and a low-Cu VVER-1000 RPV weld (SV10KhGNMAA, 0.04% Cu) (Ulbricht et al., 2023) was reported. The irradiation temperature, average neutron fluence and neutron flux were 255°C, 140×10^{18} cm^{-2}, 5.5×10^{12} cm^{-2} s^{-1} (E > 0.5 MeV), respectively for JRQ and JPA. For the VVER-1000 weld, the corresponding values were 255°C, 65×10^{18} cm^{-2}, 4.1×10^{12} cm^{-2} s^{-1}, respectively. These studies have in common post-irradiation annealings at 350°C/10 h. The degrees of recovery of $\Delta HV10$ derived from the reported data are summarized in Table 9. It is found that, despite the much shorter annealing as compared to the present study (10 h versus 100 h), the degree of recovery of $\Delta HV10$ is higher (VVER-1000 weld as compared to weld SG-4) or comparable (JRQ and JPA as compared to base metal GW-

TABLE 9 Recovery of ΔHV10 derived from reported values after annealing at 350°C/10 h. The irradiation temperature was 255°C, the neutron flux was in the range 2.8–5.4 × 10^{12} cm^{-2} s^{-1} (E > 0.5 MeV). Divide fluence by 1.5 to get an approximation of the fluence for neutron energies E > 1 MeV.

Material	Neutron fluence, E > 0.5 MeV (10^{18} cm^{-2})	Recovery of ΔHV10 η (%)
A533B cl. 1, JRQ	139	17 ± 5
A533B cl. 1, JPA	80	15 ± 7
VVER-1000 weld	65	17 ± 8

8). While for the latter two the higher Cu content may play a role, the dominant factor for the more efficient recovery of VVER-1000 weld as compared to weld SG-4 is certainly the lower irradiation temperature and the resulting larger difference between annealing and irradiation temperature of 95 K. Fabry et al. (1984) reported results on the annealing at 343°C/672 h of A302B-type RPV plate steel neutron-irradiated at 274°C. Based on ΔTT, the degree of recovery was estimated to be less than 50%, which is consistent with the degree of recovery obtained from the small punch test in the present study.

Finally, it is worth referring to a SANS study of two neutron-irradiated RPV welds during *in situ* annealing (Boothby et al., 2015). The reported weld is characterized by a low Ni content (0.08 wt%) but artificially high Cu content (0.56 wt%). It was irradiated at 250°C up to a neutron fluence of approximately 5×10^{18} n/cm² (E > 1 MeV), that means, one order of magnitude less than for GW-8 of the present study. Based on the reported data, post-irradiation annealing at 347°C/0.5 h resulted in 9% and 15% recovery in terms of volume fraction and number density, respectively. Taking into account the different Cu contents, irradiation conditions, and annealing times as compared to the present SANS study, these degrees of recovery are in a reasonable proportion with the results listed in Table 7.

5 Conclusion

The experimental data presented for an annealing temperature of $T = 343$°C extend an existing data base on the recovery of neutron-irradiated RPV steels at annealing temperatures representative of wet annealing. The included VVER-440 base metal was irradiated at a relatively high temperature of 290°C and experienced a high neutron flux, while the irradiation conditions of the VVER-440-type weld (270°C, low flux) are representative of the real pressure vessel. The added value is particularly associated with the covered range of annealing times from 100 up to 2,000 h. The data indicate a progressing recovery at increasing annealing time instead of a saturation. Moreover, a multitude of methods was applied to independently estimate degrees of recovery while managing with the limited amount of available material. The large method-to-method variability of the degree of recovery partly results from statistical errors and is partly due to the different details revealed by the applied methods as indicated above.

It is neither the objective of this study nor possible to recommend wet annealing in any particular case. On the one hand, a broader data base is required. On the other hand, archive material runs out. As a learnt lesson, small-specimen test techniques and the re-use of existing material, e.g., SANS followed by Vickers hardness on the same samples, are beneficial.

Data availability statement

The datasets presented in this study can be found in online repositories. The names of the repository/repositories and accession number(s) can be found below: https://doi.org/10.14278/rodare.3006.

Author contributions

EA: Writing–review and editing, Conceptualization, Data curation, Formal Analysis, Funding acquisition, Investigation, Methodology, Project administration, Supervision. FB: Conceptualization, Data curation, Formal Analysis, Funding acquisition, Methodology, Project administration, Supervision, Writing–original draft, Writing–review and editing. J-EB: Data curation, Formal Analysis, Investigation, Writing–review and editing. PC: Data curation, Formal Analysis, Investigation, Methodology, Writing–review and editing. JD: Data curation, Formal Analysis, Investigation, Writing–review and editing. MH: Data curation, Formal Analysis, Methodology, Writing–review and editing. AU: Data curation, Formal Analysis, Investigation, Writing–review and editing.

Conflict of interest

The authors declare that the research was conducted in the absence of any commercial or financial relationships that could be construed as a potential conflict of interest.

Publisher's note

All claims expressed in this article are solely those of the authors and do not necessarily represent those of their affiliated organizations, or those of the publisher, the editors and the reviewers. Any product that may be evaluated in this article, or claim that may be made by its manufacturer, is not guaranteed or endorsed by the publisher.

References

Ahlstrand, R., Klausnitzer, E. N., Lange, D., Leitz, C., Pastor, D., and Valo, M. (1993). "Evaluation of the recovery annealing of the reactor pressure vessel of NPP nord (Greifswald) units 1 and 2 by means of subsize impact specimens," in *Radiation Embrittlement of nuclear reactor pressure vessel steels: an international review (fourth volume), ASTM STP 1170*. Editor L. E. Steele (Philadelphia: American Society for Testing and Materials), 321–344. doi:10.1520/STP24785S

Almirall, N., Wells, P. B., Yamamoto, T., Wilford, K., Williams, T., Riddle, N., et al. (2019). Precipitation and hardening in irradiated low alloy steels with a wide range of Ni and Mn compositions. *Acta Mater* 179, 119–128. doi:10.1016/j.actamat.2019.08.027

Altstadt, E., Bergner, F., and Houska, M. (2021). Use of the small punch test for the estimation of ductile-to-brittle transition temperature shift of irradiated steels. *Nucl. Mater. Energy* 26, 100918. doi:10.1016/j.nme.2021.100918

Amayev, A. D., Kryukov, A. M., and Sokolov, M. A. (1993). "Recovery of the transition temperature of irradiated WWER-440 vessel metal by annealing," in *Radiation Embrittlement of nuclear reactor pressure vessel steels: an international review (fourth volume), ASTM STP 1170*. Editor L. E. Steele (Philadelphia: American Society for Testing and Materials), 369–379. doi:10.1520/STP24787S

Bergner, F., Ulbricht, A., Hernandez-Mayoral, M., and Pranzas, K. (2008). Small-angle neutron scattering study of neutron-irradiated iron and an iron–nickel alloy. *J. Nucl. Mater.* 374, 334–337. doi:10.1016/j.jnucmat.2007.07.008

Boothby, R. M., Hyde, J. M., Swan, H., Parfitt, D., Wilford, K., and Lindner, P. (2015). SANS examination of irradiated RPV steel welds during *in-situ* annealing. *J. Nucl. Mater.* 461, 45–50. doi:10.1016/j.jnucmat.2015.02.036

Brumovsky, M. (2015) "Embrittlement of reactor pressure vessels (RPVs) in WWER-type reactors," in *Irradiation embrittlement of reactor pressure vessels (RPVs) in nuclear power plants*, Amsterdam: Woodhead Publishing Series in Energy, 107–131. doi:10.1533/9780857096470.2.107

Brumovsky, M., Ahlstrand, R., Brynda, J., Debarberis, L., Kohopää, J., Kryukov, A. M., et al. (2008). *Annealing and re-embrittlement of reactor pressure vessel materials, AMES Report No. 19, European Project ATHENA*.

Dewhurst, C. D., Grillo, I., Honecker, D., Bonnaud, M., Jacques, M., Amrouni, C., et al. (2016). The small-angle neutron scattering instrument D33 at the Institut Laue–Langevin. *J. Appl. Cryst.* 49, 1–14. doi:10.1107/S1600576715021792

Dudarev, S. L. (2022). Grand challenges in nuclear engineering. *Front. Nucl. Eng.* 1, 945270. doi:10.3389/fnuen.2022.945270

Fabry, A., Motte, F., Stiennon, G., Debrue, J., Gubel, P., Van de Velde, J., et al. (1984). Annealing of the BR3 reactor pressure vessel, in twelfth water reactor safety research information meeting. Rockville, Maryland: Proceedings of the U.S. Nuclear Regulatory Commission, NUREG/CP-0058, 4, 144–175.

Gillemot, F. (2010). Study of irradiation effects at the research reactor. *Problemy Procnosti* Kiev, Ukraine: ISSN 0556-171X, 105–111.

Glatter, O. (1980). Determination of particle-size distribution functions from small-angle scattering data by means of the indirect transformation method. *J. Appl. Cryst.* 13, 7–11. doi:10.1107/S0021889880011429

Kocik, J., Keilova, E., Cizek, J., and Prochazka, I. (2002). TEM and PAS study of neutron irradiated VVER-type RPV steels. *J. Nucl. Mater.* 303, 52–64. doi:10.1016/S0022-3115(02)00800-0

Krasikov, E. (2015). Radiation intensification of the reactor pressure vessels recovery by low temperature heat treatment (wet annealing). *IOP Conf. Ser. Mater. Sci. Eng.* 81, 012002. doi:10.1088/1757-899X/81/1/012002

Kryukov, A. (2019). "Actual issues of VVER reactor pressure vessel irradiation embrittlement assessment," in *Proceedings of the EUROSAFE 2019 Conference, Gesellschaft für Reaktorsicherheit*. Cologne: (Köln), 9–20.

Mager, T. R., Dragunov, Y. G., and Leitz, C. (1998). *Thermal annealing of an embrittled reactor pressure vessel*. Technical Report IWG-LMNPP-98/3. Vienna: International Atomic Energy Agency, International Working Group on Life Management of Nuclear Power Plants, 505–530.

Mathon, M. H., Barby, A., Dunstetter, F., Maury, F., Lorenzelli, N., and De Novion, C. H. (1997). Experimental study and modelling of copper precipitation under electron irradiation in dilute FeCu binary alloys. *J. Nucl. Mater.* 245, 224–237. doi:10.1016/S0022-3115(97)00010-X

Nanstad, R. K., Server, W. L., Sokolov, M. A., Odette, G. R., and Almirall, N. (2018). "Some useful mechanical property correlations for nuclear reactor pressure vessel steels," in *Proceedings of the ASME 2018 pressure vessels and piping conference (PVP2018)*. Article No. PVP2018–84786. doi:10.1115/PVP2018-84786

Odette, G. R., and Lucas, G. E. (1998). Recent progress in understanding reactor pressure vessel steel embrittlement. *Rad. Eff. Def. Solids* 144, 189–231. doi:10.1080/10420159808229676

Ortner, S. (2023). A review of structural material requirements and choices for nuclear power plant. *Front. Nucl. Eng.* 2, 1253974. doi:10.3389/fnuen.2023.1253974

Pachur, D. (1982). Radiation annealing mechanisms of low-alloy reactor pressure vessel steels dependent on irradiation temperature and neutron fluence. *Nucl. Technol.* 59, 463–475. doi:10.13182/NT82-A33004

Pelli, R., and Törrönen, K. (1998). On thermal annealing of irradiated PWR pressure vessels. *Int. J. Press. Vess. Pip.* 75, 1075–1095. doi:10.1016/S0308-0161(97)00078-1

Server, W. L., and Biemiller, E. C. (1993). "Recent evaluation of "wet" thermal annealing to resolve reactor pressure vessel embrittlement," in *Proceedings of the SMiRT-12 conference*. Editor K. Kussmaul DG03/5, 423–428.

Sokolov, M. A., Server, W. L., and Nanstad, R. K. (2015). "Thermal annealing of reactor pressure vessels," in *Proceedings of the ASME 2015 pressure vessels and piping (PVP) conference*. Paper ID PVP2015-45773. doi:10.1115/PVP2015-45783

Timofeev, B., Brumovsky, M., and Von Estorff, U. (2010). *Certification report of 15Kh2MFA/15Cr2MoVA steel and its welds for WWER reactor pressure vessels*. Luxembourg: Publications Office of the European Union. *Technical Report JRC57754, EUR 24581 EN*.

Ulbricht, A., Altstadt, E., Bergner, F., Viehrig, H.-W., and Keiderling, U. (2011). Small-angle neutron scattering investigation of as-irradiated, annealed and reirradiated reactor pressure vessel weld material of decommissioned reactor. *J. Nucl. Mater.* 416, 111–116. doi:10.1016/j.jnucmat.2010.12.219

Ulbricht, A., Bergner, F., Dewhurst, C. D., and Heinemann, A. (2006). Small-angle neutron scattering study of post-irradiation annealed neutron irradiated pressure vessel steels. *J. Nucl. Mater.* 353, 27–34. doi:10.1016/j.jnucmat.2006.02.083

Ulbricht, A., Dykas, J., Chekhonin, P., Altstadt, E., and Bergner, F. (2023). Small-angle neutron scattering study of neutron-irradiated and post-irradiation annealed VVER-1000 reactor pressure vessel weld material. *Front. Nucl. Eng.* 2, 1176288. doi:10.3389/fnuen.2023.1176288

Urwank, P. (1989). Unambiguous curve fitting and error estimation for Charpy impact test data of reactor pressure vessel steels suitable for a small number of samples. *J. Nucl. Mater.* 161, 24–29. doi:10.1016/0022-3115(89)90458-3

Viehrig, H.-W., Altstadt, E., Houska, M., Mueller, G., Ulbricht, A., Konheiser, J., et al. (2018). *Investigation of decommissioned reactor pressure vessels of the nuclear power plant Greifswald. Technical Report HZDR-088*, Helmholtz-Zentrum Dresden-Rossendorf.

Viehrig, H.-W., Boehmert, J., and Dzugan, J. (2002). Some issues by using the master curve concept. *Nucl. Eng. Des.* 212, 115–124. doi:10.1016/S0029-5493(01)00465-4

Viehrig, H.-W., Gillemot, F., Horvat, M., Acosta, B., and Debarberis, L. (2010). "Irradiation response of Greifswald unit 8 RPV steels," in *Proc. IAEA-JRC technical Meeting on irradiation Embrittlement and life Management of reactor pressure vessels (held oct. 2010, znojmo, Czech republic)*.

Viehrig, H.-W., Schuhknecht, J., Rindelhardt, U., and Weiss, F.-P. (2009). Investigation of beltline welding seam of the Greifswald WWER-440 unit 1 reactor pressure vessel. *J. ASTM Int.* 6, 1–10. doi:10.1520/JAI101925

Wallin, K. (1999). The master curve method: a new concept for brittle fracture. *Int. J. Mater. Prod. Technol.* 14, 342–354. doi:10.1504/IJMPT.1999.036276

Yamamoto, M., and Miura, N. (2015). "Applicability of miniature C(T) specimens for the master curve evaluation of RPV weld material," in *Proceedings of the ASME 2015 pressure vessels and piping conference (PVP2015)*. Article No. PVP2015–45545. doi:10.1115/PVP2015-45545